Submitted to ADVANCED FUNCTIONAL MATERIALS

DOI: 10.1002/adfm.((please insert DOI)

Controlling the morphology and efficiency of hybrid ZnO:polythiophene solar cells via side chain functionalization

By *Stefan D. Oosterhout*, *L. Jan Anton Koster*, *Svetlana S. van Bavel*, *Joachim Loos, Ole Stenzel*, *Ralf Thiedmann*, *Volker Schmidt*, *Bert Campo*, *Thomas J. Cleij*, *Laurence Lutzen*, *Dirk Vanderzande*, *Martijn M. Wienk*, and *René A. J. Janssen**

[*] Prof. R. A. J. Janssen, S. D. Oosterhout, Dr. M. M. Wienk, Dr. L. J. A. Koster
Molecular Materials and Nanosystems
Eindhoven University of Technology
PO Box 513
5600 MB Eindhoven (The Netherlands)
E-mail: r.a.j.janssen@tue.nl

Dr. S. S. van Bavel, Dr. J. Loos
Laboratory of Materials and Interface Chemistry and Soft Matter, CryoTEM Research Unit
Eindhoven University of Technology
PO Box 513
5600 MB Eindhoven (The Netherlands)

R. Thiedmann, O. Stenzel, Prof. V. Schmidt
Institute for Stochastics
Ulm University
D-89069 Ulm (Germany)

Dr. B. Campo, Prof. T. J. Cleij, Dr. L. Lutzen, Prof. D. Vanderzande
Hasselt University
Institute for Materials Research
Wetenschapspark 1
BE 3590 Diepenbeek (Belgium)

Keywords: Conjugated Polymers, Zinc Oxide, Solar Cells, Hybrid Materials

The efficiency of polymer – metal oxide hybrid solar cells critically depends on the intimacy of mixing of the two semiconductors. We investigate the effect of side chain functionalization on the morphology and performance of conjugated polymer:ZnO solar cells. Using an ester-

functionalized side chain poly(3-hexylthiophene-2,5-diyl) derivative (P3HT-E), the nanoscale morphology of ZnO:polymer solar cells is significantly more intimately mixed compared to ZnO:poly(3-hexylthiophene-2,5-diyl) (ZnO:P3HT) as evidenced experimentally from a three dimensional reconstruction of the phase separation using electron tomography. Photoinduced absorption reveals nearly quantitative charge generation for the ZnO:P3HT-E blend but not for ZnO:P3HT, consistent with the results obtained from solving the three dimensional diffusion equation for excitons formed in the polymer within the two experimental ZnO morphologies. For thin ZnO:P3HT-E active layers (~50 nm) this yields a significant improvement of the solar cell performance. For thicker cells, however, the reduced hole mobility and a reduced percolation of ZnO pathways hinders charge carrier collection, limiting the power conversion efficiency.

1. Introduction

By combining considerable power conversion efficiencies with desirable properties such as low weight and mechanical flexibility, thin film organic polymer photovoltaic devices are an attractive approach for generating renewable energy. The use of roll-to roll solution processing of devices adds to the prospects of obtaining efficient and low-cost devices. Moreover, the optical and electrical properties of the materials can be tuned by changing the molecular structure. This has resulted in a substantial increase in efficiency of polymer solar cells in the last few years,[1-7] where first applications are emerging.[8,9]

Photoexcitation in organic semiconductors does not lead to free charge carriers which are required for a photovoltaic effect. Instead, strongly bound electron-hole pairs (excitons) are created that will only separate into free carriers at an interface between an electron donor (*p*-type) and electron acceptor (*n*-type) material. The distance that such an exciton is able to cover is very limited, dependent on the diffusion constant of the exciton and its intrinsic

lifetime. Ideally, an exciton is created within a few nanometers of the donor-acceptor interface to ensure a high quantum efficiency of charge generation and consequently most organic solar cells are based on a bulk heterojunction in which the *n*-type and *p*-type materials are intimately mixed. Today, the most efficient organic solar cells combine *p*-type conjugated polymers with *n*-type fullerenes, reaching efficiencies up to 7.4%.[7]

An alternative to full-organic solar cells are so-called hybrid solar cells. These devices combine the solution processability of organic compounds with the morphological stability of inorganic materials, such as CdSe,[10-12] TiO_2,[13-16] or ZnO.[17-23] Recently, we achieved an power conversion efficiency (PCE) of 2.0% for a ZnO:poly(3-hexylthiophene-2,5-diyl) (ZnO:P3HT) blend, which was prepared by spin coating a mixture of P3HT and diethylzinc (DEZ) as a ZnO precursor from a common solvent.[22] During spin coating, DEZ reacts with ambient moisture to form $Zn(OH)_2$, while the solvent evaporates. By subsequent annealing of the $Zn(OH)_2$:P3HT layer to 100 °C it is possible to complete the condensation reaction of $Zn(OH)_2$ into ZnO and to form a hybrid ZnO:P3HT bulk heterojunction active layer. Due to the large polarity difference between the organic and inorganic components, phase separation occurs. For thin layers, this process affords coarsely phase separated films that limit charge generation. Thicker films obtained by spin coating at lower speed, on the other hand, are better mixed, but here charge extraction becomes limiting, because an increasing part of the ZnO is no longer connected to the electron collecting electrode, disabling part of the charges formed to contribute to the photocurrent.[22]

The challenge now, is to make hybrid layers that feature both high generation efficiency and high charge collection. This is expected to lead to higher efficiencies in ZnO:polymer hybrid solar cells. To achieve this goal we have investigated a more hydrophilic polythiophene derivative with ester-functionalized side chains.[24] The ester functions in poly[(3-hexylthiophene-2,5-diyl)-*co*-(3-(2-acetoxyethyl)thiophene-2,5-diyl)] (7:3 ratio)

(P3HT-E, **Fig. 1**) are more compatible with the polar ZnO surface. We expected it to yield more finely dispersed ZnO in the polymer matrix and, hence, an improved charge carrier generation and power conversion efficiency.

2. Results and discussion

2.1. Microscopy

ZnO:P3HT and ZnO:P3HT-E films were prepared by spin coating a mixture of the polymer and DEZ from a chlorobenzene:toluene:tetrahydrofuran solvent mixture in a N_2 atmosphere with a relative humidity of 40%, followed by annealing at 100 °C as described in detail in the experimental section. The mixed films were made with a ZnO:polymer ratio that is optimal for the performance of the solar cell (*vide infra*). This implies a somewhat larger ZnO content in the ZnO:P3HT-E compared to the ZnO:P3HT film.

The surface topographies of thin (~50 nm) ZnO:polymer films were investigated with tapping mode atomic force microscopy (TM-AFM). The spin-coated and annealed ZnO:P3HT blends shows a rough topography with a RMS surface roughness of 25 nm, which indicates a coarse phase separation (**Fig. 2a**),.[22] Using P3HT-E instead of P3HT (**Fig. 2b**), the layer shows a much smoother surface with a RMS surface roughness of only 4.7 nm, implying a better miscibility of P3HT-E and ZnO. Transmission electron microscopy (TEM) affords information about the bulk of the active layer. Owing to the high electron density in ZnO, there is a large contrast between polymer and ZnO, which makes TEM an excellent imaging technique to investigate this type of layers. The TEM image of the 50 nm thin film of ZnO:P3HT clearly shows large ZnO clusters and large pure polymer domains (**Figure 3a**). As P3HT is the only absorber of visible light in the active layer, these large P3HT domains are unfavorable because the excitons created in such domain cannot diffuse towards the interface with ZnO during their lifetime and decay before being able to form charges. In the 50 nm film

of ZnO:P3HT-E, however, ZnO is much more evenly dispersed inside the polymer matrix (**Figure 3b**). This more intimate mixing is favorable for charge generation.

To obtain a more detailed insight into the morphologies, electron tomography was performed on the 50 nm thin layers of ZnO:P3HT and ZnO:P3HT-E. The images of the reconstructed volumes are shown in **Figure 3c**, ZnO being yellow and the polymer being transparent against a black background. Note that the ZnO:P3HT-E image (**Fig. 3d**) is shown at slightly higher magnification. The images clearly confirm that ZnO much better disperses in P3HT-E than in P3HT. The volume fraction of ZnO calculated from the three dimensional morphologies that is present differs for the two films; 13 vol-% ZnO present in Zn:P3HT and 17 vol-% in ZnO:P3HT-E. We note that the composition of both films had been optimized for the solar cell performance at this layer thickness. For both films there is less ZnO present then expected based on the amount of DEZ in the solution. Assuming full conversion of all added DEZ, the ZnO content would have been 20 and 25 vol-%, respectively. In both cases, part of the DEZ evaporates during spin coating.

2.2. Spectroscopic analysis

UV/visible absorption spectra of pure films of P3HT and P3HT-E are virtually identical (**Fig. 4a,b**), indicating a similar degree of crystallization and a comparable optical band gap. In sharp contrast, the absorption spectra of the mixed ZnO:polymer films differ substantially. The ZnO:P3HT film displays an absorption spectrum that closely resembles that of the pure polymer, but the ZnO:P3HT-E film exhibits a significantly blue-shifted absorption, suggesting less pronounced polymer crystallization. This difference can be explained by an increased interaction between this polymer and ZnO and by smaller polymer domains, impeding effective aggregation.

Photoinduced absorption (PIA) spectroscopy was performed on the active layers to investigate the efficiency of charge generation. **Figure 4c** shows PIA spectra of blends of

P3HT and P3HT-E with ZnO recorded with photoexciation at 488 nm. The PIA spectrum of ZnO:P3HT shows a bleaching band from 1.9-2.5 eV, in correspondence with its neutral absorption spectrum. For ZnO:P3HT-E the bleaching band has a less well resolved vibronic progression and is located at slightly higher energy (the onset has shifted by 0.07 eV), characteristic for less crystalline polythiophene. The signals at 0.4, 1.25, and 1.8 eV in the ZnO:P3HT can be attributed to polarons (radical cations) in P3HT. The signal at 0.4 eV is overlapping with that of conduction band electrons in ZnO.[22] Importantly, the ZnO:P3HT blend shows a significant peak at 1.08 eV which can be attributed to a triplet-triplet absorption.[22,25-28] Triplets are indicative for incomplete charge generation because they result from intersystem crossing from the singlet excited state, which is a relatively slow process. The triplet-triplet ($T_n \leftarrow T_1$) absorption in polythiophenes is known to shift to lower energy upon aggregation much like the onset of the normal optical absorption ($S_1 \leftarrow S_0$).[26-28] In fact, the magnitude of the shift of $T_n \leftarrow T_1$ is almost identical to shift of the onset of $S_1 \leftarrow S_0$.[26] Because in the blends of ZnO:P3HT-E the onset has shifted by 0.07 eV, the $T_n \leftarrow T_1$ PIA would have been expected at ~1.08 + 0.07 = 1.15 eV. **Figure 4c** shows no signal at this position. The absence of a significant triplet absorption in the ZnO:P3HT-E blend indicates that virtually all singlet excitons created in P3HT-E are quenched by ZnO and afford charge separation before they can intersystem cross to the triplet state. Consistently, the contribution of the signal at 0.4 eV of electrons in ZnO has increased in ZnO:P3HT-E film. The P3HT-E polaron band is shifted towards higher energy (~1.34 eV) as a result of the reduced crystallization inferred from the position of the bleaching band. The improved charge generation for ZnO:P3HT-E will to some extend be due to a somewhat larger ZnO content, but based on the microscopy, we expect the degree of mixing to have a much larger effect.

2.3. Charge carrier generation

To quantify the effect of the coarseness of the phase separation on the charge carrier generation, the exciton diffusion in the active layers has been modeled using the three dimensional electron tomography ZnO morphologies.[22] The diffusion of the excitons in the polymer phase can be modeled by solving the diffusion equation for steady state:

$$\frac{dn}{dt} = -\frac{n}{\tau} + D\nabla^2 n + g = 0 \qquad (1)$$

where D is the diffusion constant, n is the exciton density, τ is the exciton lifetime and g is the rate of exciton generation. The exciton lifetime and diffusion rate in P3HT are taken from the literature,[29] and assumed to be equal for both P3HT and P3HT-E: τ = 400 ps and $D = 1.8 \times 10^{-7}$ m^2 s^{-1}. Furthermore, it is assumed that ZnO is a perfect quencher, consequently, n = 0 at the ZnO:polymer interface. Disregarding the effect of electrodes, using cyclic boundary conditions, this leads to a charge carrier generation efficiency of 40% in the ZnO:P3HT blend, and to 96% in the ZnO:P3HT-E blend. This is illustrated in **Figure 5** and summarized in **Table 1**. It has been reported that the excitons can also be quenched at electrodes like PEDOT:PSS and Al.[30-32] This quenching, however, will not contribute to the photocurrent. When quenching at the electrodes is taken into account in the exciton diffusion modeling, ca. 32% of the excitons in ZnO:P3HT are quenched at the electrodes and only ca. 32% of the excitons afford charge carriers (**Table 1**). The remaining excitons are lost via intrinsic decay. For ZnO:P3HT-E, still 90% of the excitons yield charge carriers, while only 5.8% are quenched at the electrodes. This clearly demonstrates that the significantly improved charge carrier generation obtained for a finer phase separation also decimates possible exciton losses at the electrodes.

2.4. Percolation pathways in ZnO

Besides charge carrier generation, also charge collection is essential. This may be limited, especially by discontinuities in the ZnO percolation network which has a volume percentage of less than 20%.[22] The three dimensional electron tomography data were analyzed to determine the fraction of ZnO connected to the aluminum top electrode where electrons are collected and the fraction of ZnO connected via a monotonously rising path. The latter excludes pathways that do not continue in the direction towards the collecting electrode where electrons may become trapped and recombine before being collected. The results are summarized in **Table 1**. The fraction of ZnO connected to the aluminum electrode is near unity for both ZnO:polymer active layers. The fraction connected via monotonously rising path is significantly lower for the ZnO:P3HT-E film, but still quite high at 81%. Looking at the combined effects of charge carrier generation and connectivity we would expect larger currents in ZnO:P3HT-E compared to ZnO:P3HT.

2.5. Solar cell performance

Photovoltaic devices have been fabricated by sandwiching a 50 nm thick ZnO:polymer layer between glass\ITO\PEDOT:PSS and evaporated aluminum contacts. The ZnO content of the active layer was varied to gain optimum power conversion efficiency, leading to 13 vol-% ZnO in the ZnO:P3HT layer, whereas the ZnO:P3HT-E devices exhibited this maximum at 17 vol-%, as determined by electron tomography on the photoactive layers of actual devices. Current density - voltage (*J-V*) characteristics and external quantum efficiency (EQE) measurements are shown in **Figure 6**. Typical parameters are summarized in **Table 2**. Comparing the two 50 nm layer devices, the cell with P3HT-E has a higher open circuit voltage (V_{oc}) and short circuit current (J_{sc}) than the P3HT device, while the fill factor (FF) is lower. The high V_{oc} for P3HT-E is attributed to the larger optical band gap, as shown in the absorption (**Fig. 4b**) and EQE (**Fig. 6b**) onset, while the comparatively low V_{oc} for thin P3HT

is likely caused by the presence of shunts that arise when the layer roughness (25 nm RMS, *vide supra*) is on the order of the layer thickness (50 nm). These shunts also cause the strongly increased (dark) current for the 50 nm ZnO:P3HT below -0.5 V (Fig 6a). The larger current for P3HT-E is ascribed to the increase in charge carrier generation in the active layer resulting from the more intimate mixing.

ZnO:P3HT devices significantly improve by increasing the active layer thickness to 120 nm (**Table 2**), resulting from fewer shunts and thus a higher V_{oc}, and improved currents, owing to a better mixing.[22] On the other hand, when a thicker ZnO:P3HT-E active layer (~120 nm) is produced, the J_{sc} does not increase, despite the increased absorption of light. Charge carrier generation calculations were not available for this layer, because three dimensional electron tomography was not possible due to the fine phase separation. However, in the PIA spectrum of a thick ZnO:P3HT-E layer (not shown) no triplets were observed, indicating quantitative charge carrier generation. Therefore, charge collection must be a serious loss factor for these devices. Also at reverse bias (-2 V) the photocurrent of the 120 nm ZnO:P3HT-E cell remains less than that of the ZnO:P3HT cell, showing that at higher reverse electric fields the additional carriers are not yet collected.

Ternary mixtures of ZnO:P3HT:P3HT-E did improve the performance. For a range of film thicknesses between 50 and 120 nm, 1:1 mixtures of P3HT:P3HT-E gave very similar performance in combination with ZnO as P3HT-E.

A critical parameter for collection is the charge carrier mobility. The hole mobilities in the pure polymers and ZnO:polymer blends were determined in hole-only devices which were fabricated by sandwiching a neat polymer or ZnO:polymer layer between PEDOT:PSS and gold electrodes. In these devices, the space charge limited current can be described by the Mott-Gurney law (equation 2).[33]

$$J = \frac{9}{8}\varepsilon_0\varepsilon_r\mu\frac{V^2}{L^3}\exp\left(0.891\gamma\sqrt{\frac{V}{L}}\right) \quad (2)$$

Where the applied voltage V_{app} has been corrected for the built-in voltage (V_{bi}) originating from the work function difference between the electrodes and for the series resistance (V_{rs}), which is mainly the resistance over the ITO contact such that $V = V_{app} - V_{bi} - V_{rs}$. Further, μ is the hole mobility in the sandwiched layer, ε_0 the permittivity of vacuum, ε_r the weighted average dielectric constant of the two components, and γ the field activation parameter. By fitting the experimental *J-V* curve, the hole mobility was determined. The results are summarized in **Table 3**. The hole mobility found for P3HT was 2×10^{-8} m^2 V^{-1} s^{-1}, which is consistent with literature values.[34] The hole mobility found for neat P3HT-E is in the same order of magnitude. When P3HT is blended with ZnO, the mobility decreases with about one order of magnitude. This effect is strongly enhanced in blends of P3HT-E with ZnO where hole mobilities are 3 to 5 orders of magnitude lower than in the pure P3HT-E. We note that the hole-only devices of the blends exhibited a noticeable built-in voltage (0.5 V for ZnO:P3HT-E and 0.3 V for ZnO:P3HT), therefore injection of electrons into the LUMO of the ZnO cannot completely be excluded. Consequently, the measured values for the hole mobility of blends are maximum values.

It has been demonstrated before that the morphology affects hole mobility. A finer morphology leads to lower mobilities and solar cell efficiencies, because of more complicated pathways for charges.[35-37] Besides the morphology, also crystallinity is of importance, as polythiophenes are known to have higher hole mobility in the crystalline state with a lamellar organization of polymer chains .[38,39] Crystallinity is indicated by a red-shift in absorption compared to the amorphous material. The blue-shifted absorption for ZnO:P3HT-E indicates

a lower crystallinity for this polymer when mixed with ZnO (**Fig. 4b**). This is likely due to interaction with the ZnO surface and/or the extended interface area between the two materials.

3. Conclusions

Using an ester-functionalized P3HT-E that has a better compatibility towards the hydrophilic ZnO a dramatic change in the morphology of the mixed bulk-heterojunction ZnO:polymer film has been obtained compared to P3HT that lacks these groups functional. The use of P3HT-E leads to a much finer phase separation when blended with ZnO, and hence, a higher surface area for exciton dissociation and charge carrier generation between the two materials. The fraction of large polymer domains has decreased significantly using P3HT-E compared to P3HT, leading to nearly quantitative charge carrier generation within the blend. The more intimate mixing in ZnO:P3HT-E, however, seems to reduce the ZnO connectivity and due to a lower degree of crystallinity the hole mobility decreases compared to the reference compound, P3HT. Therefore, only in thin devices, the current and power conversion efficiency is enhanced.

4. Experimental

Regioregular P3HT (M_n = 30 kg/mol with a polydispersity of 2.1) was obtained from Rieke Metals. Before use, it was reduced using hydrazine and purified using soxhlet extraction with hexane and chloroform. Regioregular P3HT-E (M_n = 21 kg/mol with a polydispersity of 2.1) was prepared following the Rieke method.[24] Poly(3,4-ethylenedioxythiophene):poly (styrene sulfonate) (PEDOT:PSS) was purchased from H.C. Stark (Clevios P VP.AI 4085) and filtered over a 5 μm filter before use. Aluminum wire was used for evaporation and purchased from Alfa Aesar, DEZ was purchased from Sigma-Aldrich (1.1 M solution in toluene).

Polymer:DEZ solutions were prepared by mixing a known amount of polymer with the appropriate amount of chlorobenzene and DEZ stock solution (0.4 M, obtained by the addition of a 1.1 M DEZ solution (1.8 mL) in toluene dry tetrahydrofuran (to 3.2 mL)). The correct amount of stock solution, leading to the desired vol-% ZnO in the active layer, assuming full conversion of the DEZ into ZnO, was added and chlorobenzene was added to yield an overall polymer concentration of 10 mg mL^{-1}.

Substrates for device preparation were glass plates covered with patterned tin-doped indium oxide (ITO). These substrates were thoroughly cleaned by sonication in acetone and aqueous dodecyl sulfate solution, followed by rinsing with water and sonication in isopropanol. Finally UV-ozone was applied for 30 min. After this step, the substrates were transferred to a nitrogen-filled glove box with a controlled relative humidity of 40%. PEDOT:PSS was spin coated at a spin speed of 3000 rpm for one minute, followed by annealing on a hot plate for 15 min. at 100 °C. Then, the active layer was spin coated from the solution described above; with the spin speed adjusted to the desired layer thickness for one minute, and was subsequently dried at 3000 rpm for one minute. The layer was aged for 15 min. and heated at 100 °C for 15 min. to form the ZnO and anneal the polymer. The substrates were then transferred to a glove box with an inert nitrogen atmosphere (<1 ppm H_2O and <1 ppm O_2) using an air-tight container. The back electrode, consisting of 100 nm aluminum, was evaporated under high vacuum ($<3 \times 10^{-7}$ mbar). For hole-only devices a layer of 80 nm gold was evaporated instead. All subsequent handling and analysis of the cells was carried out under an inert atmosphere.

J-V characteristics were measured using a Keithley 2400 Source Meter, controlled by a computer. The device was illuminated by a 50 W tungsten-halogen lamp filtered by a Schott GG420 UV filter and a Hoya LB120 daylight filter. External quantum efficiency measurements were performed with respect to a calibrated silicon reference. A homebuilt set-

up utilizing a Philips focusline 7027 light source and an Oriel monochromator was used. The devices were exposed to bias illumination during the EQE measurement, using a 530 nm laser, to emulate the charge carrier density in the device that would occur at 1000 W m^{-2} AM 1.5 conditions. The monochromatic and laser light was focused on an aperture with a diameter of 2 mm, to create a light spot smaller than the device area. Convoluting the EQE spectrum with the AM1.5 spectrum yields the J_{sc}, which was in good correspondence (within 20 %) of the J_{sc} measured using the tungsten-halogen lamp.

Atomic force microscopy (AFM) was applied on the devices using a Veeco MultiMode with a Nanoscope III controller, in tapping mode. The used probes were PPP-NCH-50 from Nanosensors. The thicknesses of the layers were determined using a Veeco Dektak 150 surface profiler.

For TEM investigations, the P3HT:ZnO films were floated from the water soluble PEDOT:PSS substrate onto the surface of demineralized water and picked up with 200-mesh copper TEM grids. Bright-field TEM morphology observation and acquisition of tilt series for electron tomography were performed on a Technai G^2 20 TEM (FEI Co.) operated at 200 kV. All tilt series were obtained in an automatic fashion by using EXPLORE 3D software (FEI Co.), in the tilt range of ±70º with a saxton tilt scheme with a 0º tilt step of 1.5º. The alignment and (SIRT-)reconstruction of the data series was performed by using INSPEC 3D (FEI Co.) and visualization of the 3D reconstructed volume was done with Amira 4.1 (Mercury Computer Systems, Inc.). For the statistical analysis with GeoStoch (Institute of Stochastics, Ulm University) and exciton diffusion modeling the electron tomography data were binarized.

Photoinduced absorption (PIA) measurements were carried out using a homebuilt setup, by exciting a part of the device where no ITO or metal electrode is present, inside a continuous flow cryostat at 80 K with a mechanically modulated (275 Hz) Ar-ion laser

(Spectra Physics 2025) pump beam at 488 nm (25 mW, beam diameter of 2 mm). The resulting change in transmission of a tungsten-halogen white-light probe beam was monitored after dispersion by a triple-grating monochromator, using Si, InGaAs, and a cooled InSb detector using lock-in amplifiers.

Acknowledgements

The research was supported by a TOP grant of the Chemical Sciences (CW) division of the Netherlands Organization for Scientific Research (NWO) and is part of the Joint Solar Programme (JSP). The JSP is co-financed by the Foundation for Fundamental Research on Matter (FOM), Chemical Sciences of NWO and the Foundation Shell Research. This work was further supported by the Deutsche Forschungsgemeinschaft under Priority Programme 1355 'Elementary Processes of Organic Photovoltaics'. The research was further supported by the "Europees Fonds voor Regionale Ontwikkeling" (EFRO) in the Interreg IV-A project Organext.

Received: ((will be filled in by the editorial staff))
Revised: ((will be filled in by the editorial staff))
Published online: ((will be filled in by the editorial staff))

References

_[1] B. C. Thompson, J. M. J. Fréchet, *Angew. Chem. Int. Ed.* **2008**, *47*, 58.

_[2] J. Peet, J. Y. Kim, N. E. Coates, W. L. Ma, D. Moses, A. J. Heeger, G. C. Bazan, *Nat. Mater.* **2007**, *6*, 497.

_[3] R. C. Coffin, J. Peet, J. Rogers, G. C. Bazan, *Nat. Chem*. **2009**, *1*, 657.

_[4] S. H. Park, A. Roy, S. Beaupre, S. Cho, N. Coates, J. S. Moon, D. Moses, M. Leclerc, K. Lee, A. J. Heeger, *Nat. Photonics* **2009**, *3*, 297

_[5] Y. Liang, D. Feng, Y. Wu, S. Tsai, G. Li, C. Ray, L. Yu, *J. Am. Chem. Soc.* **2009**, *131*, 7792.

_[6] J. C. Bijleveld, A. P. Zoombelt, S. G. J. Mathijssen, M. M. Wienk, M. Turbiez, D. M. de Leeuw, R. A. J. Janssen, *J. Am. Chem. Soc.* **2009**, *131*, 16616

_[7] Y. Liang, Z. Xu, J. Xia, S. Tsai, Y. Wu, G. Li, C. Ray, L. Yu, *Adv. Mater.* **2010**, E135.

_[8] R. Gaudiana, C. Brabec, *Nat. Photon.* **2008,** *2*, 287.

_[9] F.C. Krebs, T.D. Nielsen, J. Fyenbo, M. Wadstrøm, M.S. Pedersen, *Energy Environ. Sci.* **2010**, *3*, 512.

_[10] W. U. Huynh, J. J. Dittmer, A. P. Alivisatos, *Science* **2002**, *295*, 2425.

_[11] P. Wang, A. Abrusci, H. M. P. Wong, M. Svensson, M. R. Andersson, N. C. Greenham, *Nano Lett*. **2006**, *6*, 1789.

_[12] S. Dayal, N. Kopidakis, D. C. Olson, D. S. Ginley, G. Rumbles, *Nano Lett.* **2010**, *10*, 239.

_[13] C. Y. Kwong, A. B. Djurisic, P. C. Chui, K. W. Cheng, W .K. Chan, *Chem. Phys. Lett.* **2004**, *384*, 372.

_[14] C. Y. Kuo, W. C. Tang, C. Gau, T. F. Guo, D. Z. Jeng, *Appl. Phys. Lett.* **2008**, *93*, 033307.

_[15] Y.-Y. Lin, T.-H. Chu, S.-S. Li, C.-H. Chuang, C.-H. Chang, W.-F. Su, C.-P. Chang, M.-W. Chu, C.-W. Chen, *J. Am. Chem. Soc.* **2009**, 131, 3644.

_[16] G. K. Mor, S. Kim, M. Paulose, O. K. Varghese, K. Shankar, J. Basham, C. A. Grimes, *Nano Lett.* **2009**, *9*, 4250.

_[17] W. J. E. Beek, M. M. Wienk, R. A. J. Janssen, *Adv. Mater.* **2004***, 16*, 1009.

_[18] W. J. E. Beek, M. M. Wienk, R. A. J. Janssen, *Adv. Funct. Mater.* **2006**, *16*, 1112

_[19] D. C. Olson, Y. Lee, M. S. White, N. Kopidakis, S. E. Shaheen, D. S. Ginley, J. A. Voigt, J. W. P Hsu, *J. Phys. Chem. C* **2007**, *111*, 16640.

_[20] D. J. D. Moet, L. J. A. Koster, B. de Boer, P. W. M. Blom, *Chem. Mater.* **2007**, *19*, 5856.

_[21] F. C. Krebs, Y. Thomann, R. Thomann, J. W. Andreasen, *Nanotechnology*, **2008**, *19*, 424013.

_[22] S. D. Oosterhout, M. M. Wienk, S. S. van Bavel, R. Thiedmann, L. J. A. Koster, J. Gilot, J. Loos, V. Schmidt, R. A. J. Janssen, *Nat. Mater.* **2009**, *8*, 818.

_[23] S. Wu, Q. Tai, Y. Feng, *J. Phys. Chem. C* **2010**, *114*, 6197.

_[24] B. Campo, *PhD Thesis*, **2009**, Hasselt University (Belgium).

_[25] P. A. van Hal, M. P. T. Christiaans, M. M. Wienk, J. M. Kroon, R. A. J. Janssen, *J. Phys. Chem. B* **1999**, *103*, 4352.

_[26] See supporting information of: D. Veldman, S. C. J. Meskers, R. A. J. Janssen, *Adv. Funct. Mater*. **2009**, *19*, 1939.

_[27] M. P. T. Christiaans, B. M. W. Langeveld-Voss, R. A. J. Janssen, *Synth. Met.* **1999**, *101*, 177.

_[28] J. J. Apperloo, R.A. J. Janssen, P. R. L. Malenfant, J. M. J. Fréchet, *J. Am. Chem. Soc.* **2001**, *123,* 6916.

_[29] P. E. Shaw, A. Ruseckas, I. D. W. Samuel, *Adv Mater.* **2008,** *20*, 3516.

_[30] H. Becker, S. E. Burns, R. H. Friend, *Phys. Rev. B* **1997**, *56*, 1893.

_[31] K. Yim, R. Friend, J. Kim, *J. Chem. Phys.* **2006**, *124*, 184706.

_[32] D. E. Markov, P. W. M. Blom, *Phys. Rev. B* **2005**, *72*, 161401 (R).

_[33] P. N. Murgatroyd, *J. Phys. D* **1970**, *3*, 151.

_[34] V. D. Mihailetchi, H. X. Xie, B. de Boer, L. J. A. Koster, P. W. M. Blom, *Adv. Func. Mater*. **2006**, *16*, 699.

_[35] C. Groves, L. J. A. Koster, N. C. Greenham, *J. Appl. Phys.* **2009**, *105*, 094510.

_[36] L. J. A. Koster, *Phys. Rev. B* **2010**, *81*, 205318.

_[37] R. G. E. Kimber, A. B. Walker, G. E. Schröder-Turk, D. J. Cleaver, *Phys. Chem. Chem. Phys.* **2010**, *12*, 844

_[38] F. Padinger, R. S. Rittberger, N. S. Sariciftci, *Adv. Func. Mater.* **2003**, *13*, 85.

_[39] G. Li, V. Shrotriya, J. Huang, Y. Yao, T. Moriarty, K. Emery, Y. Yang, *Nat. Mater.* **2005**, *4*, 864.

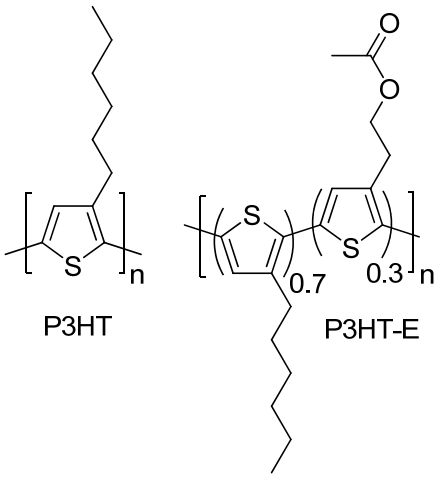

Figure 1. Molecular structures of P3HT and P3HT-E.

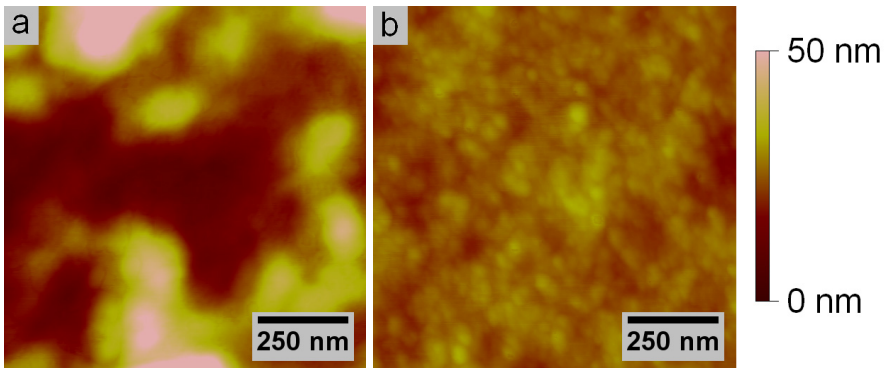

Figure 2. AFM height images of ZnO:P3HT (a) and ZnO:P3HT-E (b) active layers.

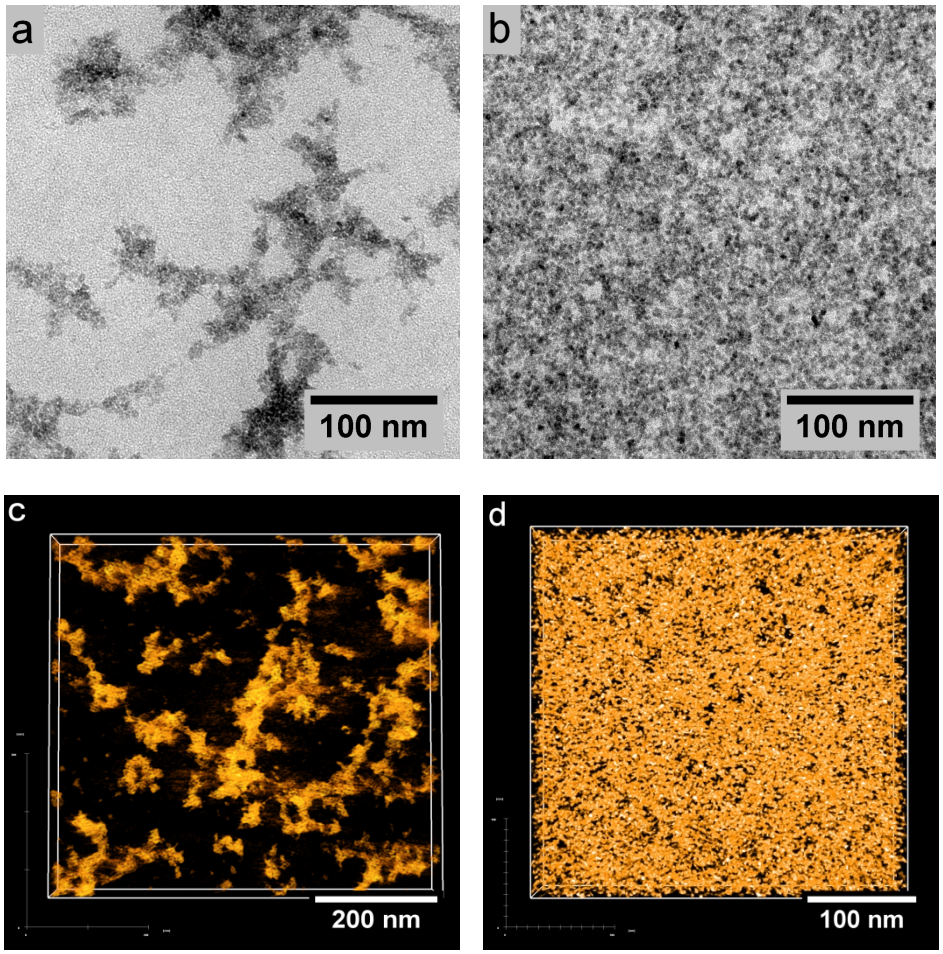

Figure 3. TEM images of a blend layer of ZnO:P3HT (a) and ZnO:P3HT-E (b), and the reconstructed volumes from electron tomography of ZnO:P3HT (c) and ZnO:P3HT-E (d).

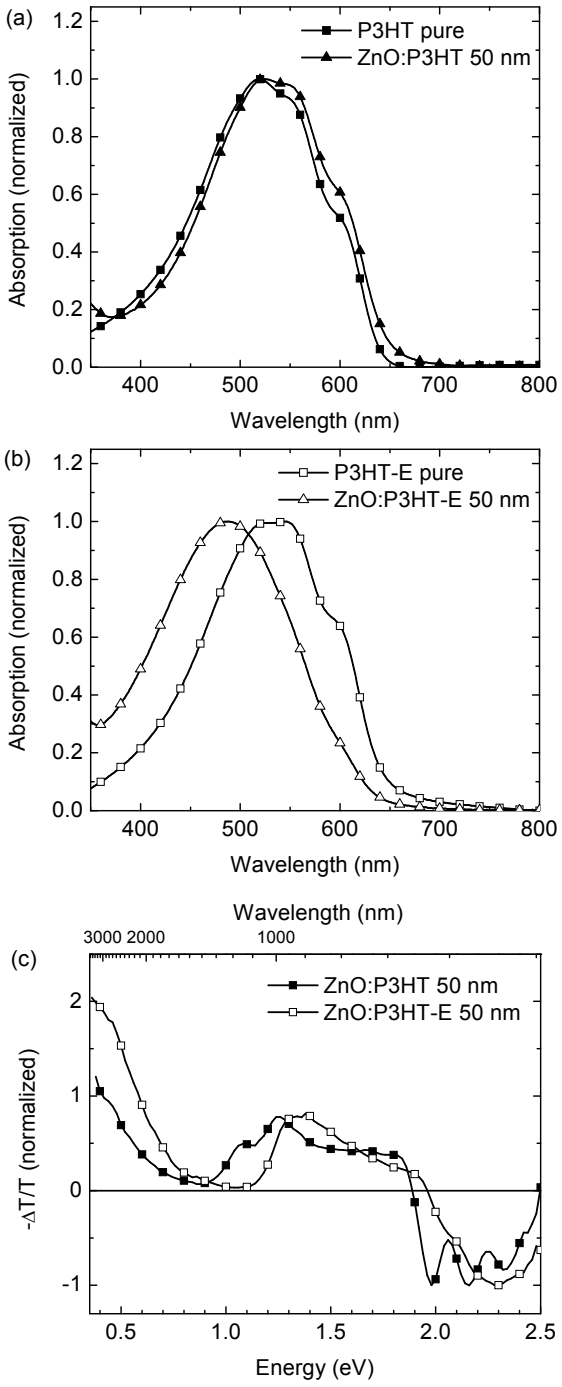

Figure 4. Normalized absorption, measured in transmission, of pure polymers and the respective blends with ZnO for P3HT (a) and P3HT-E (b). Photoinduced absorption spectra of ZnO:P3HT and ZnO:P3HT-E (c).

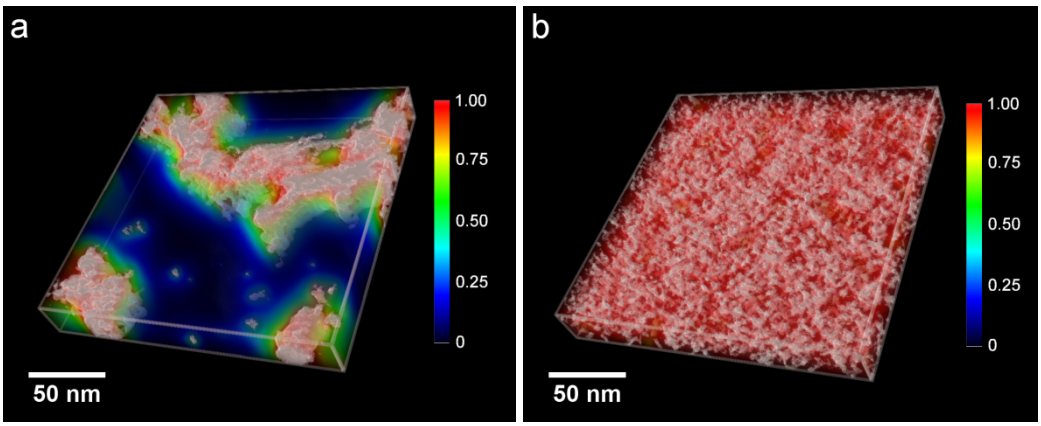

Figure 5. Calculated charge carrier generation efficiency in experimentally determined morphologies for ZnO:P3HT (a) and ZnO:P3HT-E (b). The ZnO appears white; the efficiency is indicated by the color.

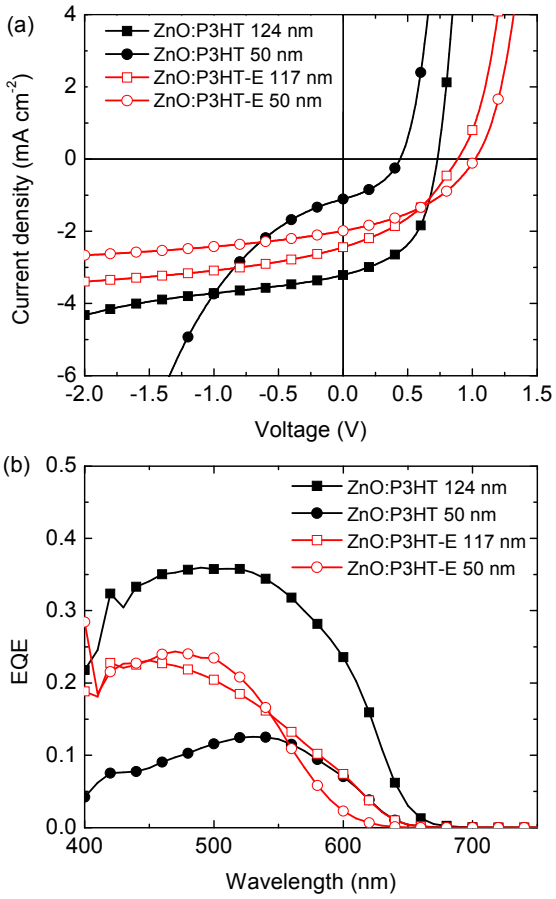

Figure 6. *J-V* (a) and EQE (b) curves of ZnO:P3HT and ZnO:P3HT-E solar cells.

Table 1. Exciton quenching and ZnO connectivity data for 50 nm films.

		Without electrodes	With electrodes			
	ZnO volume fraction [%]	Generation efficiency [%]	Generation efficiency [%]	Quenched by electrodes [%]	ZnO connected to top [%]	ZnO monotonously connected to top [%]
ZnO:P3HT	13	40	32	32	96	93
ZnO:P3HT-E	17	96	90	6	95	81

Table 2. Device parameters for ZnO:polymer cells.

Device	d [nm]	V_{oc} [V]	J_{sc} [mA cm^{-2}]	Fill factor	PCE [%]
ZnO:P3HT	124	0.75	4.3	0.53	1.7
	50	0.44	1.3	0.39	0.22
ZnO:P3HT-E	117	0.80	2.2	0.38	0.74
	50	1.02	2.1	0.40	0.83

Table 3. Hole mobilities ($m^2 V^{-1} s^{-1}$) of pure polymers and blends (±1 order of magnitude).

	P3HT	P3HT-E
Pure polymer	2×10^{-8}	5×10^{-8}
Thick blend (~120 nm)	8×10^{-10}	2×10^{-11}
Thin blend (~50 nm)	4×10^{-8}	9×10^{-13}

The efficiency of ZnO:polythiophene hybrid solar cells critically depends on the intimacy of mixing of the ZnO and the polymer. An ester functionalized polythiophene copolymer is able to greatly enhance mixing of the materials, leading to superb exciton generation efficiency, but the fine phase separation hinders charge carrier transport to the electrodes, limiting the device performance.

Keywords: Conjugated Polymers, Zinc Oxide, Solar Cells, Hybrid Materials

Stefan D. Oosterhout, L. Jan Anton Koster, Svetlana S. van Bavel, Joachim Loos, Ole Stenzel, Ralf Thiedmann, Volker Schmidt, Bert Campo, Thomas J. Cleij, Laurence Lutzen, Dirk Vanderzande, Martijn M. Wienk, and René A. J. Janssen*

Controlling the morphology and efficiency of hybrid ZnO:polythiophene solar cells via side chain functionalization